JOURNAL OF PROPULSION AND POWER
Vol. 22, No. 3, May–June 2006

Flow Measurements of Vortex Generator Jets in Separating Boundary Layer

L. Hansen* and J. Bons†
Brigham Young University, Provo, Utah 84602

Vortex generator jets (VGJs) have been found to be an effective method of active separation control on the suction side of a low-pressure turbine (LPT) blade at low Reynolds numbers. The flow mechanisms responsible for this control were studied and documented to provide a basis for future improvements in LPT design. Data were collected using a stereo particle-image-velocimetry system that enabled all three components of velocity to be measured. First, steady VGJs were injected into a laminar boundary layer on a flat plate (nonseparating boundary layer) to more fully understand the characteristics and behavior of the produced vortices. Jets injected normal to the surface created vortices of lesser strength that migrated out farther from the boundary layer. The vortices produced by angled jets (injected at 30-deg pitch and 90-deg skew angles to the freestream) remained closer to the wall and maintained their structure for a longer distance. The angled jets also produced vortices that were more effective at sweeping low momentum fluid up from the boundary layer while transporting high-momentum freestream fluid down towards the wall. Second, pulsed VGJs were injected on a flat plate with an applied adverse pressure gradient equivalent to that experienced by an LPT blade. This configuration was used to study the effectiveness of the flow control exhibited by both jet configurations on a separating boundary layer. Time-averaged results showed similar boundary-layer separation reduction for both normal and angled jets; however, individual characteristics of the control differed. Normal jets created a disturbance that provided flow control earlier during the pulsing cycle, whereas the disturbance produced by the angled jets was more effective in reducing the boundary-layer separation.

Nomenclature

B	=	jet blowing ratio (U_j/U_e)
C_x	=	axial chord, m
c_p	=	pressure coefficient [Eq. (1)]
d	=	jet hole diameter (4 mm)
F^+	=	nondimensional forcing frequency ($=0.41fC_x/U_{\text{in}}$)
f	=	frequency, Hz
L	=	plate length, m
L_{ss}	=	suction surface length, m
P	=	pressure, Pa
Re_{Cx}	=	inlet Reynolds number ($\rho U_i C_x/\mu$)
Re_{Lss}	=	exit Reynolds number ($\rho U_e L_{\text{ss}}/\mu$)
Re_q	=	momentum thickness Reynolds number ($\rho U_\infty \theta/\mu$)
T	=	forcing period, s
t	=	time, s
U_j	=	jet velocity, m/s
U_∞	=	freestream velocity, m/s
x	=	streamwise direction, m
y	=	wall-normal direction, m
z	=	spanwise direction
Γ	=	integrated boundary-layer momentum flux loss coefficient [Eq. (3)]
δ	=	boundary-layer thickness, m
θ	=	boundary-layer momentum thickness, m
μ	=	dynamic viscosity, kg/m · s
ρ	=	density, kg/m^3
ϕ	=	integrated wake pressure loss coefficient [Eq. (2)]

Subscripts

e	=	local boundary-layer edge
ex	=	tunnel exit
i	=	tunnel inlet
s	=	static
tot	=	total
w	=	wake
0	=	uncontrolled ($B = 0$ case)

I. Introduction

LOW-PRESSURE turbine (LPT) blades must be carefully designed to perform well under demanding operating conditions. They require a very aggressive turning angle to provide maximum power during takeoff and sufficient power for auxiliary systems during flight. At very high altitudes, the flight Reynolds number drops significantly, which can produce a laminar boundary layer along the surface of the blade. This laminar boundary layer is susceptible to separation, a condition that greatly diminishes the efficiency of the turbine. For example, Sharma[1] reported an increase in blade loss coefficient of 300% as a result of the boundary-layer separation.

Much research has been conducted to find a method of reducing the laminar boundary-layer separation in LPTs. Lake et al.[2] determined that a modification of the actual blade surface (for example, by adding dimples) successfully decreased the separation-induced losses. Volino[3] experimented with two-dimensional spanwise bars, which act as boundary-layer trips and thus prevent suction surface separation. However, passive methods of flow control such as these can inhibit proper turbine performance at design conditions and/or increase blade heat transfer. Active methods of flow control, although more difficult to implement, are preferred as they can be adapted in flight according to the current flight conditions. One such method of active flow control is the use of vortex generator jets (VGJs) to inject a small amount of airflow into the separating boundary layer. It has been suggested that VGJs cause the separated boundary layer to reattach by mixing high-momentum freestream fluid with low-momentum boundary-layer fluid.[4] This process of freestream entrainment effectively reenergizes the flow and reduces the incurred losses. For example, Sondergaard et al.[5] deduced that

Received 5 October 2004; revision received 22 September 2005; accepted for publication 25 September 2005.

*Research Assistant, CB 131; lch3@et.byu.edu. Member AIAA.
†Associate Professor, Department of Mechanical Engineering, CTB 435; jbons@byu.edu. Senior Member AIAA.

the use of VGJs reduced the separation induced wake losses by up to 60%. A further improvement was suggested by Bons et al.[6] They found that pulsing the VGJs produced a comparable reduction in boundary-layer separation, while employing only a fraction of the mass flow necessary for steady flow VGJs. This greatly decreases the amount of air that must be redirected from the compressor, thus reducing the overall losses of the entire turbine engine. These initial findings indicate that VGJs have great potential to improve the efficiency of low-pressure turbines. However, before VGJs can be successfully implemented in LPT design, a more thorough understanding of the physical mechanisms involved in the reduction of the boundary layer must be obtained. Eldredge and Bons[7] performed detailed flow measurements of steady VGJs. Their findings support the freestream entrainment theory by showing that the streamwise vortical structures caused by the steady VGJs are the dominant feature in the flow control. This result is corroborated by the detailed flow measurements of Johari and Rixon[8,9] for steady and unsteady jet injection into a turbulent boundary layer. Though their experiments are conducted without a freestream pressure gradient (and thus without separation), streamwise vortices are clearly evident in both studies.

Complementary to these experimental studies are the time-accurate computational-fluid-dynamics calculations performed by Postl et al.[10,11] They explored the effects of both steady and pulsed VGJs introduced on a flat wall with the proper applied streamwise pressure gradient. Their results suggest that the mechanisms responsible for reattachment are distinct for the steady and pulsed jets. Steady VGJs were shown to reduce separation by momentum entrainment of the streamwise vortices. It was found, however, that the pulsed VGJs tripped the flow to turbulent and introduced a two-dimensional, spanwise, unsteady wave into the flow. The effect of the jet injection angle was also studied in their work. They suggested that for the steady VGJs a skewed injection angle of 90 deg to the freestream flow (with low pitch angle) was more effective than normal injection because it increases freestream entrainment. However, for pulsed VGJs the opposite was found to be true because normal jets were more effective in the formation of spanwise vorticity than angled jets (for the same blowing ratio).

Although extensive research has been conducted on the mechanisms involved in steady VGJ flow control, and analytical studies have been performed on pulsed VGJs, there are still many unanswered questions. For instance, Bons et al.[12] documented the effect of reducing the duty cycle of jet forcing and discovered a considerable phase lag in the relaxation of the suction surface boundary layer as it returned to its separated state. The fluid mechanics responsible for this phase lag are as yet unclear. Volino[13] also studied the effect of oscillating (synthetic) VGJs on boundary-layer separation and observed the presence of streamwise vortices. In addition, Volino suggested that the disturbance caused by these vortices produced behavior very similar to that of turbulent spots, as the leading edge of the disturbance traveled faster than the trailing edge. A calmed region that was resistant to separation followed the disturbance. Thus, the different roles of boundary-layer transition and freestream entrainment in LPT separation control must still be sorted out. As such, more detailed flow analyses are necessary to establish a basis for future analytical models for LPT design. This is the objective of this research. Two different methods were used to explore the behavior of the VGJs in this study. First, both steady and pulsed VGJs were injected into a laminar boundary layer on a flat plate. The relative simplicity of this flow allowed for a better characterization of the development and movement of the jet vortices. Then, pulsed VGJs were injected into a separating boundary layer on a flat plate with an applied streamwise pressure gradient comparable to that experienced by LPT blades. This configuration enabled the previously determined vortex behavior to be used to investigate its effect on a separating boundary layer.

II. Experimental Facility

Experiments were performed in a low-speed wind tunnel that allows thermally controlled operation at tunnel velocities in excess of 20 m/s. Background freestream turbulence levels in the test section are below 0.3%, and flow uniformity is ±2%. An acrylic test section

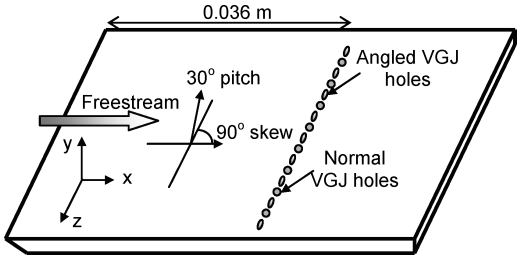

Fig. 1 Flat-plate test-section schematic.

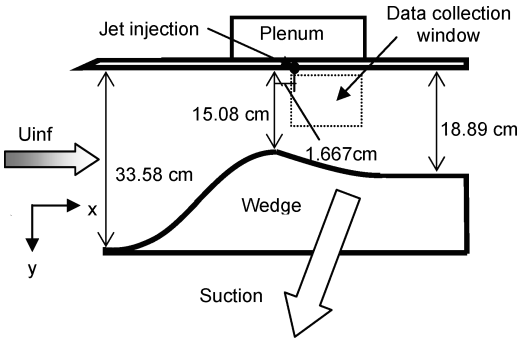

Fig. 2 Flat plate with applied streamwise pressure gradient test-section schematic.

was prepared to allow for optical access to the flow. The modular wind-tunnel construction allows the streamwise pressure gradient and wall curvature to be independently varied. Figure 1 shows the flat-plate test section. A boundary-layer bleed is employed at the leading edge to create a new, laminar boundary layer. A row of 4-mm-diam (d) cylindrical holes was created to introduce the VGJs: vertical holes aligned normal to the freestream direction and angled holes with 30-deg pitch and 90-deg skew angles. These angles were shown by Johnston[4] to be in the range where VGJs are most effective in reducing flow separation. The holes are placed approximately 10 diameters apart at 0.36 m from the boundary-layer bleed. The holes were drilled through a 2-cm-thick acrylic sheet and have a length-to-diameter ratio of 5 and 10 for the normal and angled holes, respectively. To create a streamwise pressure gradient without modifying the wall curvature, a wedge was inserted into the wall opposite the flat plate (Fig. 2). Suction was applied near the trailing edge of the wedge to ensure proper diffusion of the main flow and facilitate separation on the flat-plate test section. For this configuration, the length-to-diameter ratio of the VGJ holes was modified to 3.75 and 7.5, respectively, for the normal and angled holes.

Three-dimensional flow measurements were made using a LaVision three-component stereo particle-image-velocimetry (PIV) system. This system was mounted on a three-axis traverse located below the transparent acrylic test section to enable a full mapping of the flowfield. An Nd:YAG laser illuminated the flowfield with a light sheet approximately 1 mm in thickness. The flow was seeded with oil ($C_{26}H_{50}O_4$) particles that were 1–2 μm in diameter. Images were recorded by two digital cameras with a resolution of 1376 pixels by 1040 pixels. This provided an available data collection window of about 70 mm (y, wall normal) by 90 mm (x, streamwise). The collection window was positioned to include the region $-1 < x/d < 21$ and $1 < y/d < 16$ (approximately). The nearest wall distance was determined by first taking an image of a ruler positioned flush to the wall. This image indicated the length of the gap between the wall and the edge of the data collection window. Once the velocity vectors were calculated, the distance between the edge of the data collection window and the first velocity vector was added to the initial gap length. For the steady VGJs, the cameras and lasers were synchronized internally; however, the pulsed VGJs required that the cameras and lasers be externally synchronized to the pulsed VGJ flow.

To collect the data, the laser sheet was oriented in the x–y plane. Forty separate images (each image consisting of four individual

frames) at each z location were recorded, processed, and averaged. Averaging with more than 40 images showed no perceptible improvement in the resultant mean vector fields. The pulsed jet measurements were phase locked with the jet forcing, while the steady jet measurements were taken at an internal framing rate of 9.9 Hz. Vector processing was first completed using 64×64 pixel interrogation windows, with subsequent processing refinements resulting in vectors for every 16×16 pixels in the camera frame. The use of two cameras (stereo PIV) allowed the measurement of u, v, and w components of velocity. This procedure was repeated at increments of 2 mm in z to generate a three-dimensional block of velocity data. Vorticity components were then calculated from this data block using centered differences to approximate the velocity gradients. LaVision states the uncertainty of the seed particle displacement determination to be on the order of 0.1 pixels, depending on how easily a peak can be found in the cross correlation function. This uncertainty in displacement corresponds to a velocity uncertainty of less than 0.1 m/s (roughly $\pm 3\%$ of the freestream velocity).

III. Results

A. Flat Plate, No Streamwise Pressure Gradient, Steady Jet Injection

For the steady jet cases, the constant freestream velocity U_∞ was set so that the momentum thickness Reynolds number Re_θ at the VGJ location was $Re_\theta \cong 150$. This ensured adequate boundary-layer maturity at the point of jet injection while avoiding the critical Reynolds number (200) associated with instability growth and transition for laminar flow over a flat plate. The steady jet blowing ratio ($B \equiv$ mean jet velocity divided by local freestream velocity) was set to a value of two because this was the lowest steady mass flow required for effective control in the study by Bons et al.[6]

1. Normal Injection

Contour maps of streamwise and wall-normal velocity and the out-of-plane (streamwise) vorticity, plotted in z–y planes at 10 diameters downstream from the jet injection point, are shown in Fig. 3. Velocities are normalized by U_∞, and data were taken over two hole pitches. The reader is referred to Fig. 1 for the orientation of the Cartesian axes. $x/d = 0$ is at the centerline of the hole row, $y/d = 0$ is at the wall, and $z/d = 0$ is at the center of the hole. Several important characteristics of the flow are evident from Fig. 3. First, the lobes of low u-velocity fluid are interpreted to be the jet fluid, which is injected with no streamwise momentum (Fig. 3a). This low-velocity lobe gradually moves out from the wall as it travels downstream, ultimately reaching a maximum y/d position of 4.5 (wall distance to the center of the lobe) at $x/d = 20$. The jet trajectory is evident in Fig. 4a. Because there is zero skew to the injection, the jet remains at the same z position throughout its trajectory (Fig. 4b). Likewise observed from Fig. 3 is the development of streamwise vortices. The v/U_∞ contour plot (Fig. 3b) shows that these vortices develop as fluid is forced outward normally from the wall at the jet injection point and then cycled back towards the wall on both sides. Figure 3c shows that this effect is promulgated downstream as the double vortex grows in size while decreasing in magnitude. After traveling 15 diameters downstream, the magnitude of the vorticity is reduced by 75% (see Fig. 4b). This double vortex induces the expected mushroom-shaped u/U_∞ contour visible in Fig. 3a, as documented by Khan and Johnston.[14]

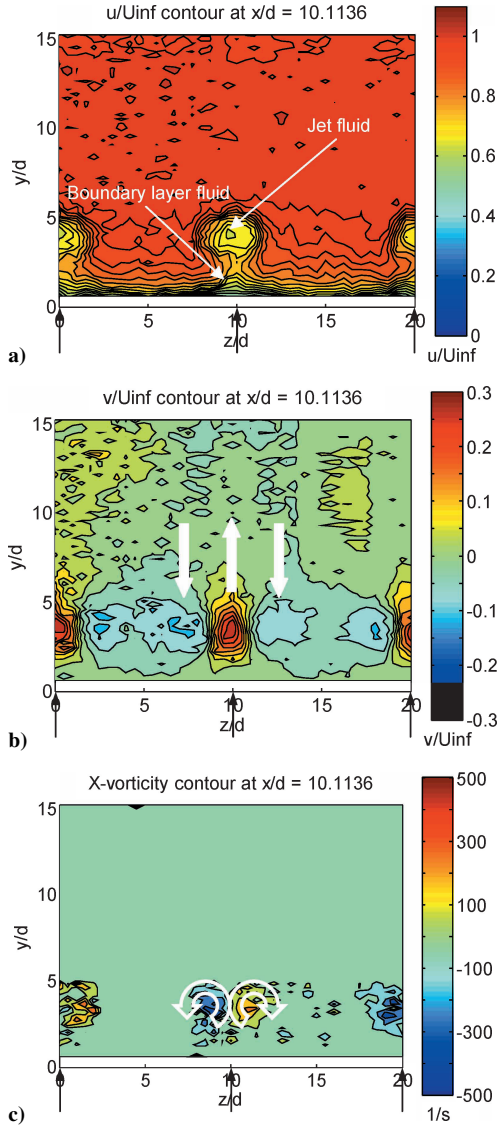

Fig. 3 Contour maps at $x/d = 10$ looking in the positive x direction for a) streamwise velocity, b) wall-normal velocity, and c) out-of-plane (streamwise) vorticity. Steady, normal jet injection into zero pressure gradient with $B = 2$. Black arrows indicate jet injection points.

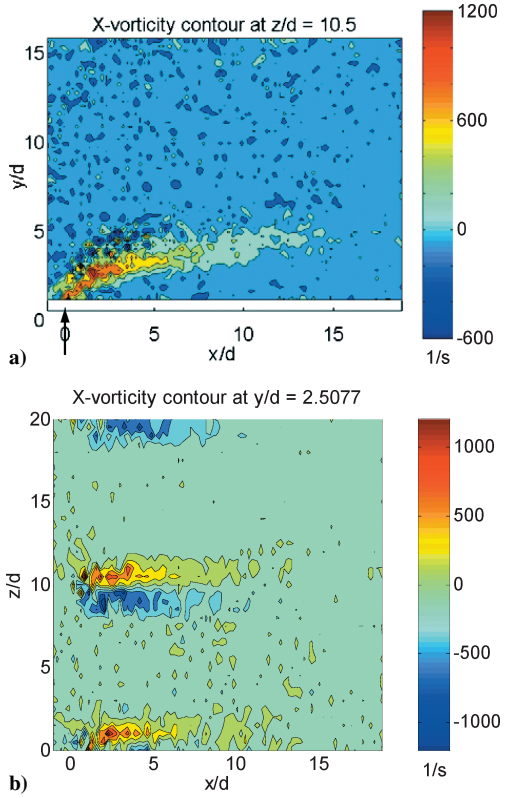

Fig. 4 Streamwise vorticity contours shown in the a) xy plane (at $z/d \approx 10$, looking in the negative z direction) and b) xz plane (at $y/d = 2.5$, looking in the positive y direction). Steady, normal jet injection into zero pressure gradient with $B = 2$.

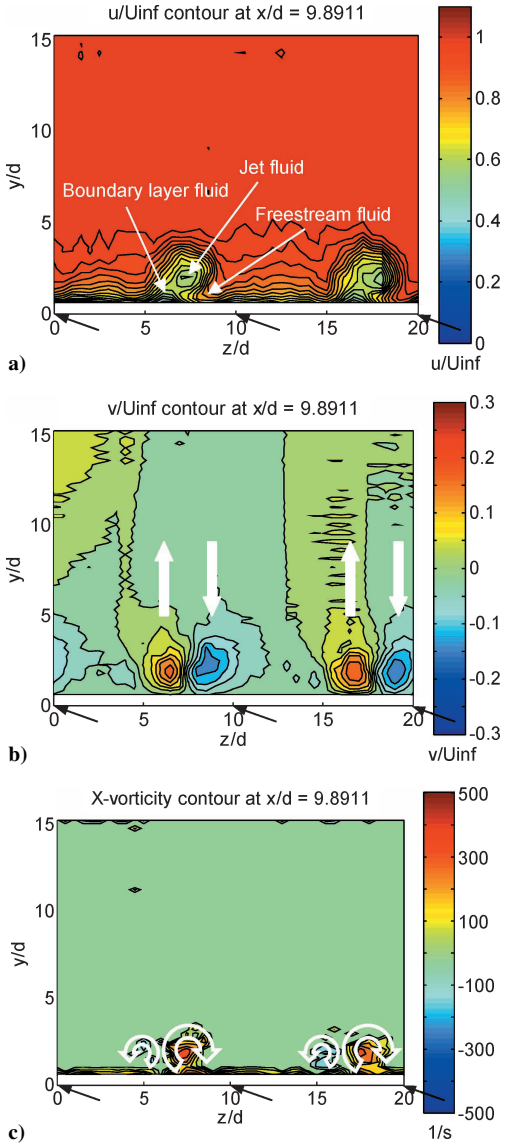

Fig. 5 Contour maps at $x/d = 10$ looking in the positive x direction for a) streamwise velocity, b) wall-normal velocity, and c) out-of-plane (streamwise) vorticity. Steady, angled jet injection into zero pressure gradient with $B = 2$. Black arrows indicate jet injection points.

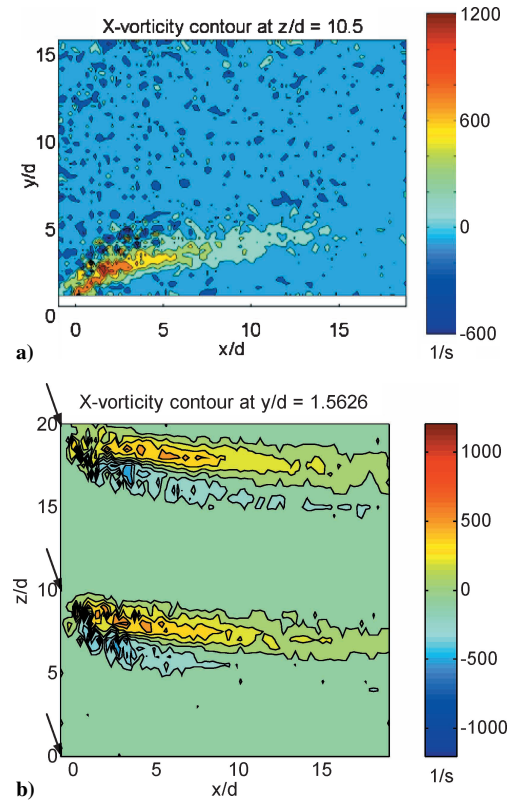

Fig. 6 Streamwise vorticity contours shown in the a) xy plane (at $z/d = 8$) and b) xz plane (at $y/d = 1.5$). Steady, angled jet injection into zero pressure gradient with $B = 2$.

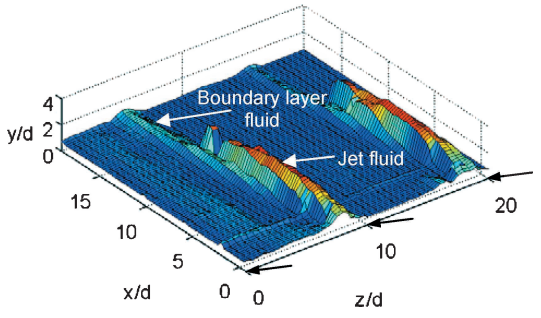

Fig. 7 Three-dimensional surface of streamwise velocity, where $u = 0.6\,U_\infty$. Steady, angled jet injection into zero pressure gradient with $B = 2$.

2. Angled Injection

Similar results were obtained for the angled jets. Figure 5 again shows streamwise and wall-normal velocity and out-of-plane (streamwise) vorticity contours in the z–y plane at the same downstream location of $x/d = 10$. Figure 6 shows the corresponding x–y and x–z planes of streamwise vorticity. The velocity is again normalized by the freestream value. As before, lobes of low u-velocity fluid (Fig. 5a) indicate the presence of jet fluid, but it is clear that the trajectory of the angled jet is different from that of the normal jet. Because of the angle of injection, the jet fluid penetrates only half as far out from the wall as the normal jet, the center of the jet fluid reaching a maximum y/d of only 2.25 at $x/d = 20$. There is, however, considerable migration in the spanwise direction, as the jet fluid travels to a position over three diameters in z from the injection point (Fig. 6b). The development of streamwise vortices is also apparent from Figs. 5 and 6. The angled jet creates a double vortex, with the dominant positive vortex becoming much stronger and larger than the negative vortex (Fig. 5c). It is clear that the vortex caused by the angled jets migrates significantly in the spanwise direction, as fluid is forced out from the wall at $z/d = 2.5$ from the injection point and then circulates back towards the wall (Fig. 5b). As in the case of normal injection, the vortex grows in size as it travels downstream. However, the primary vortex caused by the angled jets is a coherent structure for a longer distance. At a distance of 15 diameters downstream, the magnitude of the vorticity is reduced by only 45% (Fig. 6a). Both the trajectory of the primary vortex and the logarithmic streamwise decay of peak vorticity found in this research are comparable to the results of Rixon and Johari.[8]

Another phenomenon of interest is displayed more clearly in a three-dimensional plot of the flowfield. Figure 7 shows the surface where the u-velocity component is 60% of the freestream velocity ($u/U_\infty = 0.6$). It is generated by traversing the three-dimensional space of velocity data in the negative y direction from the freestream to the wall. The surface is then identified as the first occurrence of $u/U_\infty = 0.6$. The jet injection location is indicated by arrows along the z axis, and the ensuing vortical effect is evident as the flow travels downstream. The plot is colored by surface height in the y direction. The dominant characteristic of Fig. 7 is the double hump-like feature that develops downstream of each jet exit. The larger of the humps is interpreted to be the low-velocity jet fluid. After the fluid exits the hole, obstructing the freestream flow, it is gradually entrained by the main flow. By $x/d = 14$, the lobe of jet fluid has been accelerated to above 60% U_∞, and its presence in the

surface contour in Fig. 7 disappears. A second low-velocity hump located closer to the wall extends further in the x direction. This is indicative of boundary-layer fluid being drawn out from the wall. The streamwise vortices caused by the angled jets occur sufficiently close to the wall so that they pull low-momentum fluid up from the boundary layer. This behavior is also evident in Fig. 5a, where a small pocket of low-velocity fluid can be seen rising up from the wall at the position where the vortex has its highest outward movement ($z/d \approx 6.5$). Likewise, the return motion of the cycling vortex brings high-momentum freestream fluid back down close to the wall on the other side (at $z/d \approx 8.5$). This behavior is consistent with the findings of Khan and Johnston,[14] who likewise discovered a thinning and thickening of the boundary layer on opposite sides of the vortex. The high-momentum fluid brings with it turbulent fluctuations generated by the jet shear layers, creating the ingredients for flow transition in the wake of the jet (as discussed by Volino).[13]

B. Flat Plate, No Streamwise Pressure Gradient, Pulsed Jet Injection

The effect of pulsed, angled jets was also investigated. A high-pressure air line was connected to a Parker–Hannefin pulsed valve to create a pulsed jet of air. The valve was operated at a frequency of 5 Hz with a duty cycle of 25%. This jet was fed into the plenum shown in Fig. 2 to produce modulated air through the five center jet holes only. At the valve discharge into the plenum, the air pulse is essentially a step function. Some attenuation occurs in the plenum resulting in a slightly modified jet waveform as shown in Fig. 8. This figure shows the jet hole exit blowing ratio time history as measured with a single-element hot wire positioned at the jet exit (with no freestream flow). The $t/T = 0$ station represents the time at which the control signal was sent to the pulsed valve. The peak value of B is approximately 2.5, and the mean value is 0.75 for this case. PIV data were collected at eight points within the jet period and over one hole pitch (from $-7 \le z/d \le 3$). Again, 40 phase-locked images were averaged at each location. The timing of these points is also shown in Fig. 8 and was selected to obtain data during the beginning, middle, and end of the pulse, as well as during the time that the pulse was off.

As in the case of steady injection, vortices develop when the jets are pulsed. Evidence of this is shown in Fig. 9, in which a contour map of the streamwise component of velocity is displayed, colored by height in y (similar to Fig. 7). The surface represents the position at which $u/U_\infty = 0.5$ and was taken during the second phase of the pulsing cycle (while the jet is on). As in Fig. 7, the jet fluid is clearly seen entering the flowfield at the injection point. Likewise the second hump is seen at the left of the jet fluid, as the vortex sweeps the boundary-layer fluid out from the wall during its rotation. After the jet has been turned off (shown in Fig. 10), the absence of jet fluid indicates that the jet fluid introduced into the flow during the "ON" portion of the pulsing cycle (as seen in Fig. 9) has traveled downstream and is no longer visible in the data collection area. The vortex has also traveled farther downstream; however, the ensuing disruption in the boundary layer is still evident in the downstream portion of Fig. 10.

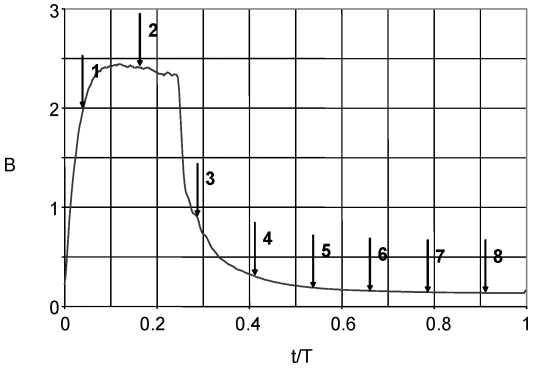

Fig. 8 Jet hole exit blowing ratio time history for VGJ operation at 5 Hz and 25% duty cycle. Arrows indicate PIV data collection points.

These results, both for the steady and pulsed jets, lend validity to the freestream entrainment theory for the application of angled jets with no freestream pressure gradient. The structure and migration of the streamwise vortices indicate that high-momentum freestream fluid is brought down close to the wall, effectively energizing the low-momentum boundary layer. However, these observations are for a nonseparating boundary layer. This leads to the following questions: 1) How does the previously discussed development of streamwise vortices affect boundary-layer separation? 2) Is the jet development altered by the decelerating flow? The following section describes the efforts made to answer these questions.

C. Flat Plate, Streamwise Pressure Gradient, Pulsed Jet Injection

The test setup was modified in order to introduce both normal and angled pulsed jets into a separating boundary layer. The wedge shown in Fig. 2 established a freestream velocity profile similar to that found on a Pack B suction surface at a low Reynolds number. The wedge design is similar to that used by Volino and Hultgren,[15] who documented its performance using a pressure coefficient c_p based on the tunnel exit velocity:

$$c_p = 1 - (U_e/U_{\text{ex}})^2 \tag{1}$$

Figure 11 shows a plot of this parameter vs the streamwise distance x normalized by the test section (suction surface) length L_{ss}, for the uncontrolled ($B = 0$) case compared to an ideal (unseparated) flow calculation.[15] Data were taken with a single-element hot wire at $y/d = 15$ and midspan. The exit Reynolds number based on L_{ss} and U_{ex} for the wedge configuration is 9×10^4. This implies an equivalent inlet Reynolds number (based on C_x and U_{in}) of 4×10^4 for the Pack B LPT blade profile used by Eldredge and Bons.[7] Using the same definition for dimensionless forcing frequency recommended in Bons et al.[12] ($F^+ = 0.41 f C_x/U_{\text{in}}$), the F^+ at 5 Hz is 0.34. The deviation in measured c_p from the ideal prediction for $0.6 < x/L_{\text{ss}} < 1$ is indicative of boundary-layer separation because

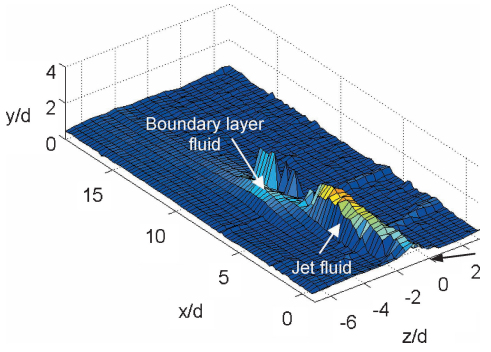

Fig. 9 Three-dimensional surface of streamwise velocity, where $u = 0.5\,U_\infty$. Data are taken during the "ON" portion of the pulsing cycle. Pulsed, angled injection into zero streamwise pressure gradient at 5 Hz and 25% duty cycle with a maximum $B = 2.5$ ($t/T = 0.15$).

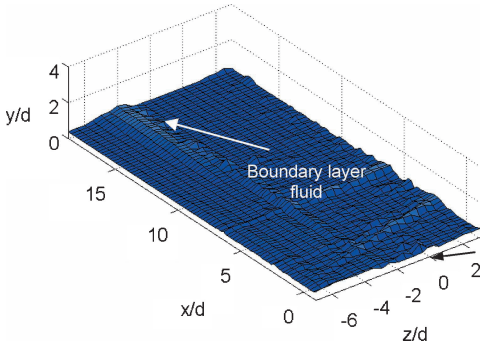

Fig. 10 Three-dimensional surface of streamwise velocity, where $u = 0.5\,U_\infty$. Data are taken during the "OFF" portion of the pulsing cycle. Pulsed, angled injection into zero streamwise pressure gradient at 5 Hz and 25% duty cycle with maximum $B = 2.5$ ($t/T = 0.40$).

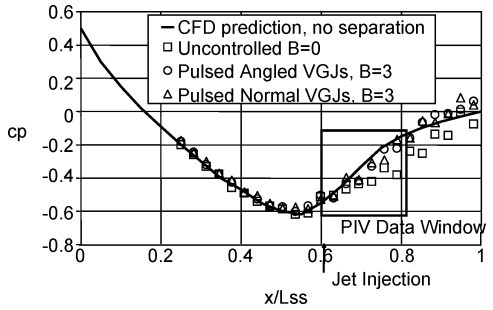

Fig. 11 Pressure coefficient distribution for wedge configuration showing uncontrolled and controlled pressure distribution in PIV data window.

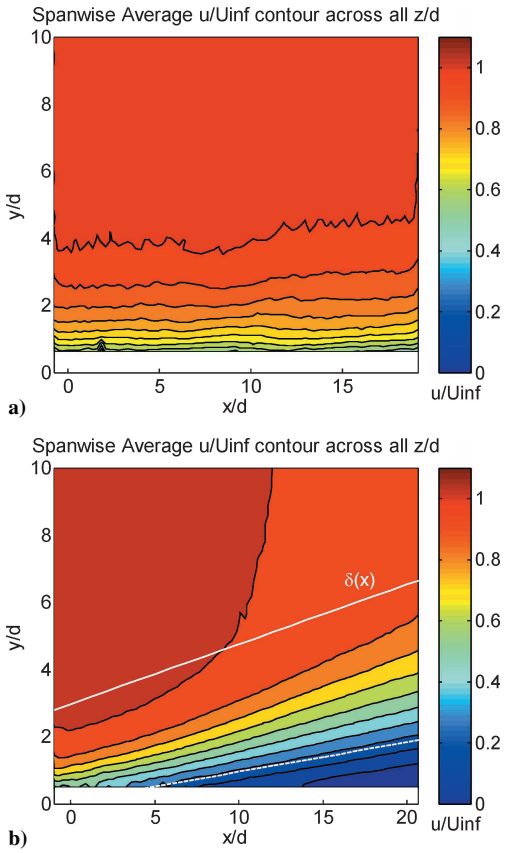

Fig. 12 Spanwise-averaged plots of the streamwise component of velocity for the uncontrolled ($B = 0$) cases: a) no pressure gradient and b) applied pressure gradient. Plots are shown looking in the negative z direction.

the desired flow deceleration is not achieved. Also shown in Fig. 11 are the c_p measurements for pulsed VGJs. The correction of flow separation is evident. The maximum B for this case was three, compared to the value of two, which was used for the zero-pressure gradient data. However, the jet exit velocity history was similar to that shown in Fig. 8.

PIV images were taken at 21 z locations over one hole pitch for this low-Reynolds-number (separated) case. The boundary-layer development for the uncontrolled cases ($B = 0$) is shown in Fig. 12, both for the flat plate (zero pressure gradient) and flat plate with the wedge inserted (applied streamwise pressure gradient). These contour plots are produced by averaging the x–y planes at all 21 z/d locations into a single plot. The effect of the presence of the inserted wedge is apparent in Fig. 12. For the wedge case (Fig. 12b), the streamwise deceleration of the freestream flow produces a rapid increase in the boundary-layer thickness and a near-wall region of low-momentum (separated) fluid (note dashed white line at $u/U_\infty = 0.2$). By comparison, the boundary layer for the no-wedge flow (Fig. 12a) shows little perceptible streamwise development. The difference in the $x/d = 0$ boundary-layer thickness between the two plots is caused by the rapid acceleration upstream of the VGJ location in the wedge configuration.

The results of the pulsed jet tests are displayed in Fig. 13, for both normal (left column) and angled (right column) injection. The flowfield is plotted as a three-dimensional surface representing the position where $u/U_\infty = 0.5$ (similar to Figs. 9 and 10). The uncontrolled case is shown first (Fig. 13a) followed by the respective flowfields for six of the eight phases within the pulsing cycle (Figs. 13b–13g). For the uncontrolled flow, the separation zone (as denoted by the dramatic rise in the $u/U_\infty = 0.5$ surface) begins about six diameters downstream of the jet injection point and grows to a maximum thickness of about $y/d = 3$ at $x/d = 20$. Figures 13b–13g clearly display the disturbance caused by the jet and its effect on the boundary layer throughout the pulsing cycle. The jet hole location is indicated by the gray ellipse, and the approximate extent of the injected fluid is marked with a pink oval. At the start of the jet pulse (Fig. 13b), the separated region is already significantly smaller than the uncontrolled case, a residual effect of the previous jet pulse. When the pulse is on (Fig. 13c), low streamwise momentum jet fluid is shown entering at $x/d = 0$. The separated area begins about 10 diameters downstream of the jet injection point, growing to a maximum thickness of about $y/d = 2$ at the downstream end of the figure. This is the maximum extent reached by the separation zone before the next pulse traverses the entire flow domain, effectively reenergizing the boundary layer. The subsequent reduction in size of the separated zone proceeds through the remainder of the pulse (Fig. 13d) before almost completely disappearing (Fig. 13e). It is not until the final phases (Figs. 13f–13g) that the separation area begins to grow again, though it never quite reaches the uncontrolled state. The next pulsing cycle begins before the flowfield can return to the uncontrolled condition. The only significant differences between the angled and normal jets in these plots are the subtle velocity deficit area directly downstream of the normal jet disturbance (Figs. 13c and 13d) and the small zone of residual low-momentum fluid over the angled jet orifice (Figs. 13e–13g), presumably caused by a small flow disturbance over the hole.

To measure the effectiveness of VGJs, it is important to quantify the boundary-layer separation losses. Previous researchers have done this using integrated total pressure measurements across the wake of the turbine blade.[5] Because the current flat-plate test facility has no blade wake, a boundary-layer parameter comparable to the integrated wake pressure loss coefficient, ϕ [Eq. (2)], was evaluated.

$$\phi = \int_{\text{mid-passage}}^{\text{mid-passage}} \frac{P_{\text{tot},i} - P_{\text{tot},w}}{P_{\text{tot},i} - P_{s,i}}\,\mathrm{d}y \tag{2}$$

If the static pressure is assumed to be constant across the boundary layer and the total pressure in the freestream ($y > \delta$) is constant, ϕ can be written as Γ, Eq. (3), for low-speed (incompressible), steady flow. This modified version of the integrated wake loss coefficient is referred to in this study as the integrated boundary-layer momentum flux loss coefficient.

$$\Gamma = \int_0^{\delta} \frac{u_e^2 - u^2}{u_i^2}\,\mathrm{d}y \tag{3}$$

The calculation of Γ is performed at the trailing edge of the PIV data domain using the spanwise-averaged streamwise velocity data (e.g., Fig. 12). Figure 14 shows Γ normalized by Γ_0 (the loss coefficient of the uncontrolled case) for each phase of the pulsing cycle. The pulsing cycle is also shown at the bottom of the figure for ease of comparison. A complication in the interpretation of Fig. 14 is encountered because of the time lag of the flow disturbance. The loss coefficient is calculated from the data taken at the farthest downstream point of the flowfield ($x/d = 20$). Therefore, these data do not correspond in time with the jet pulse shown in the figure. For example, the loss coefficient calculated with the data taken during the first phase of the pulsing cycle is not indicative of the disturbance being caused at that moment by the initiation of the jet. Rather, it quantifies the losses associated with the preceding disturbance.

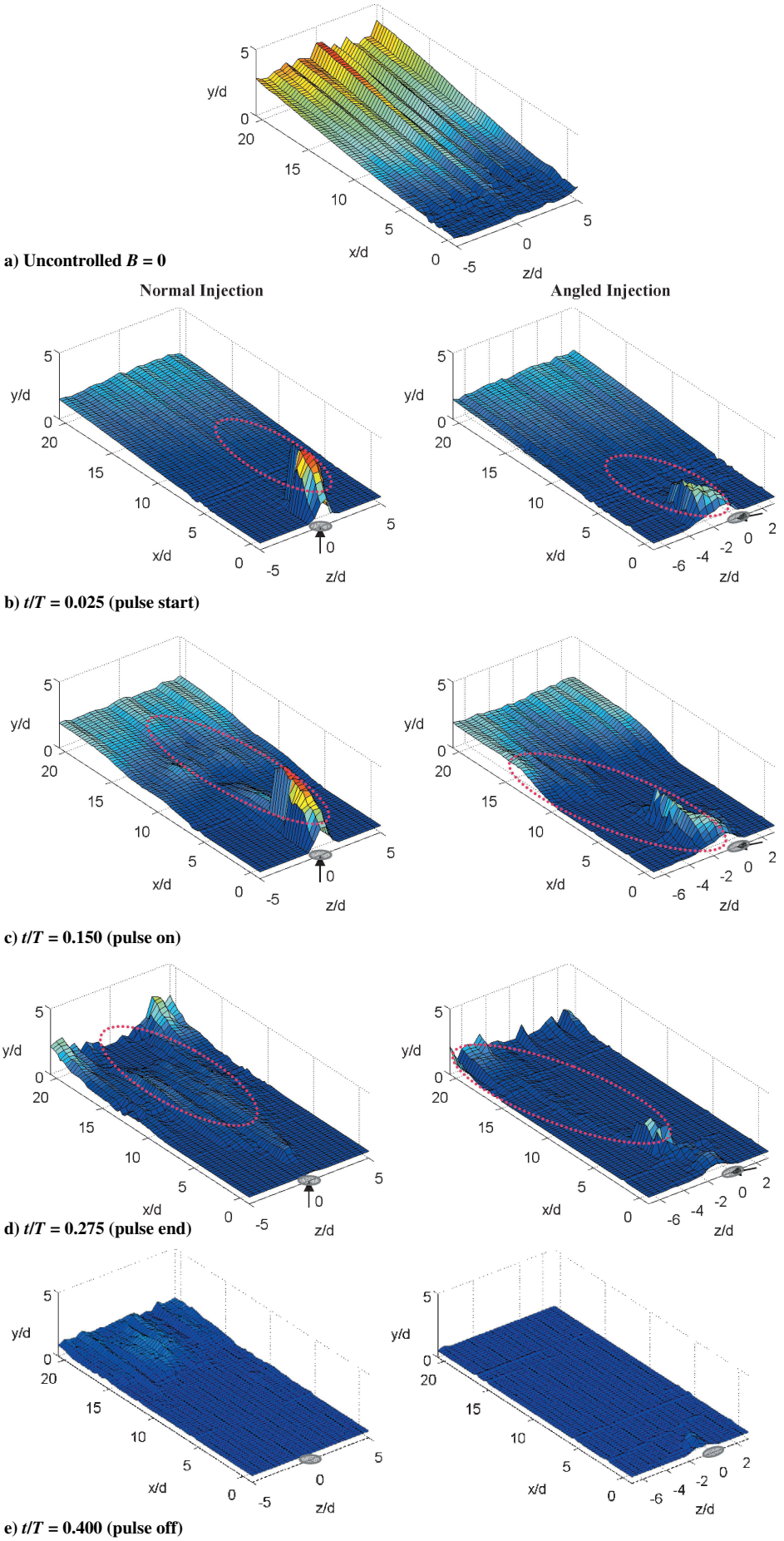

Fig. 13 Three-dimensional surface of streamwise velocity for normal (left) and angled (right) jets at $u/U_\infty = 0.5$. Gray ovals represent the VGJ holes, with black arrows indicating the presence and direction of the jet flow. Pink ovals represent the position of the jet fluid.

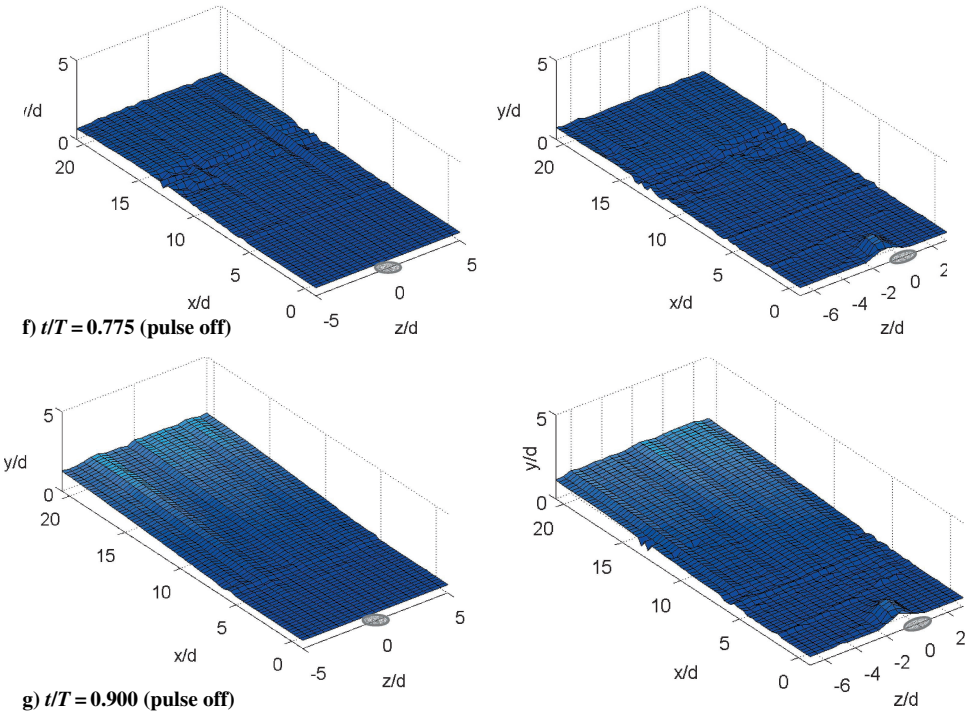

Fig. 13 Three-dimensional surface of streamwise velocity for normal (left) and angled (right) jets at $u/U_\infty = 0.5$. Gray ovals represent the VGJ holes, with black arrows indicating the presence and direction of the jet flow. Pink ovals represent the position of the jet fluid (*continued*).

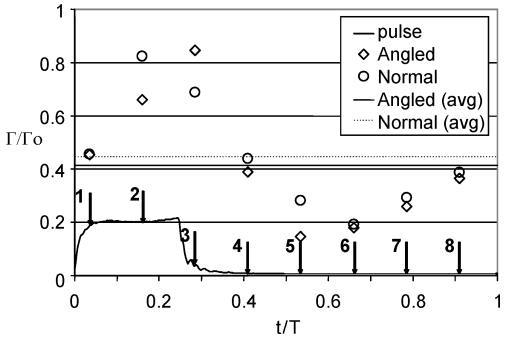

Fig. 14 Integrated boundary-layer momentum flux loss coefficient during the pulsing cycle. Normalized by the loss coefficient with $B = 0$. Pulsed injection into the wedge flow at 5 Hz and 25% duty cycle.

Though the convective time of the disturbance is difficult to quantify precisely, it is roughly equivalent to $t/T \approx 0.1$ in Fig. 14. So, the effect of the pulse shown in the lower part of the figure appears at the trailing edge ($x/d = 20$) roughly $t/T \approx 0.1$ later.

There are several observations that can be made from Fig. 14. First, there appears to be very little difference in the cycle-averaged loss coefficient for both jet orientations; each has a value slightly greater than 0.4. Although the cycle-averaged loss coefficient for the angled jets is lower than that calculated for the normal jets, the difference is small, suggesting that neither orientation has a significant advantage over the other for these flow conditions. It is also evident that the angled and normal jet configurations produce similar disturbances (as previously noted in the Fig. 13 surface plots). The loss coefficient is increasing sharply when the jet fluid enters the domain, and then decreases as the jet influence is felt downstream. The latter end of the pulsing cycle is characterized by a gradual return to uncontrolled conditions.

Of particular interest are the relative convection speeds of the disturbance. Figure 14 shows that the decline in loss coefficient calculated from the normal jets occurs sooner than the corresponding reduction from the angled jets. By phase 2, while the jet pulse is still on, the loss coefficient for the normal jets reaches a maximum and proceeds to decline during the following three phases. The angled jets do not reach a maximum loss coefficient until phase 3. This behavior is reasonable when considered in terms of the steady jet migration discussed earlier. The steady normal jets (Fig. 3) penetrated twice as far out from the wall as the angled jets (Fig. 5). Thus, the normal jets are carried out farther towards the higher-velocity freestream flow. Meanwhile, the angled jets remain closer to the wall and the low-velocity boundary-layer fluid, where they are convected downstream at a slower speed. Although the normal jet flow control is carried downstream at a faster velocity, Fig. 14 (and 13e) suggests that the angled jet flow control is more effective because it provides control of the same magnitude within a shorter period of time. This is seen by the speed at which the loss coefficient is reduced from its maximum to minimum state. The angled jets have a much steeper decline in loss coefficient, as the maximum-to-minimum reduction is completed in only two phases (phases 3–5). The normal jets, however, require four phases (phases 2–6) to reach the minimum loss coefficient. The more rapid control generated by the angled jets can be related to the stronger streamwise vorticity development observed in the steady jet data. The jet-induced boundary-layer thickening in Fig. 13d (right column) was seen previously in Figs. 7 and 10 and is evidence of streamwise vortex generation. This feature is not as prominent as it was for the flat plate case (Fig. 10), suggesting that the separating boundary layer can lift the vortex away from the wall, possibly reducing its effectiveness. The normal jet injection surface at the same t/T (Fig. 13d, left column) also shows evidence of a boundary-layer disturbance in the wake of the injected jet. In this case, the surface shows a double hump directly downstream of the jet injection location, from $6 < x/d < 16$. Clearly, this is caused by the formation of a double vortex, as seen in the steady jet data (Fig. 3). Beyond $x/d = 16$, the $u/U = 0.5$ surface is brought down to the wall, indicating strong boundary-layer reattachment before the trailing edge of the data domain. By comparison, the angled jet surface shows a much broader spatial influence of the jet vortices.

The phase-locked surfaces in Figs. 13b–13g clearly show a wave-like "flapping" of the boundary layer from attached flow to separation in response to the jet forcing frequency. However, phase-locked contour maps of spanwise vorticity viewed in the x–y plane failed to show strong evidence of the periodic, two-dimensional wave fronts (see Fig. 13) that Postl et al. predicted in their numerical simulation.[10] Their study predicted the beginning of coherent wave-like behavior during approximately the last $\frac{2}{3}$ of their computational flow domain. Because the current data collection window

equals the first $\frac{1}{3}$ of their computational domain, the data presented here cannot be used to validate the existence of these spanwise waves.

IV. Conclusions

The effect of vortex generator jets in low-Reynolds-number flows was studied. Both a flat plate (zero pressure gradient) and a flat plate with an applied pressure gradient were employed as a basis for future LPT blade experiments. The flat-plate scenario was designed to give insight into the structure and movement of the vortical structures. Steady jets were injected normally and at an angle (30-deg pitch and 90-deg skew) to the freestream flow. The normal jet created a double-vortex structure that grew in size while diminishing in strength as it traveled downstream. The vortices gradually migrated out from the wall, but maintained the same spanwise position. In contrast, the angled jet created a single vortex that migrated both up and out from the wall while remaining coherent for a longer distance than did the vortices generated by the normal jet. The vortices were observed to pull boundary layer fluid out from the wall and bring freestream fluid down close to the wall. This behavior was not as prominent when the jets were injected normally. These results show that the vortices produced by angled VGJs are structured in a way to more effectively promote freestream entrainment. Pulsed, angled jets were also applied to the flat-plate flow. The results were comparable to the steady, angled jets. The lingering boundary-layer effects caused by the streamwise vortices after the jet pulse has passed suggest that the flow control does not end immediately when the pulse is turned off.

The flat plate with an applied pressure gradient provided a separating boundary layer in which to test the effectiveness of pulsed VGJs. Normal and angled jets were again injected into the flow, and the reaction of the flow field was captured at eight discrete points in the pulsing cycle. The integrated loss coefficient was calculated to provide a quantitative basis for comparison. It was found that the cycle-averaged loss coefficient for both normal and angled jets was nearly equivalent. The normal jets initiated a disturbance to control the separation earlier in the pulsing cycle, while the angled jets produced a disturbance later in the pulsing cycle, but that reacted more quickly to control the flow. The data also suggest that the development of the streamwise vortices is modified when the jets are injected into a separating boundary layer.

Acknowledgments

The authors express appreciation to Ken Engan and Richard Eldredge for their assistance with this research; also to David Olson and Daniel Reimann for their help in constructing the wind tunnel. This work was performed under sponsorship from the Air Force Office of Scientific Research, with Thomas Beutner as contract monitor.

References

[1]Sharma, O., "Impact of Reynolds Number on LP Turbine Performance," *Proceedings of 1997 Minnowbrook II Workshop on Boundary Layer Transition in Turbomachines*, NASA/CP-1998-206958, 1998, pp. 65–69.

[2]Lake, J. P., King P. I., and Rivir, R. B., "Reduction of Separation Losses on a Turbine Blade with Low Reynolds Number," AIAA Paper 99-0242, Jan. 1999.

[3]Volino, R. J., "Passive Flow Control on Low-Pressure Turbine Airfoils," *Journal of Turbomachinery*, Vol. 125, No. 4, 2003, pp. 754–764.

[4]Johnston, J. P., "Pitched and Skewed Vortex Generator Jets for Control of Turbulent Boundary Layer Separation: A Review," *Proceedings of the 3rd ASME/JSME Joint Fluids Engineering Conference*, FEDSM99-6917, July 1999.

[5]Sondergaard, R., Bons, J. P., and Rivir, R. B., "Control of Low-Pressure Turbine Separation Using Vortex Generator Jets," *Journal of Propulsion and Power*, Vol. 18, No. 4, 2002, pp. 889–895.

[6]Bons, J. P., Sondergaard, R., and Rivir, R. B., "Turbine Separation Control Using Pulsed Vortex Generator Jets," *Journal of Turbomachinery*, Vol. 123, No. 2, April 2001, pp. 198–206.

[7]Eldredge, R. G., and Bons, J. P., 2004, "Active Control of a Separating Boundary Layer with Steady Vortex Generating Jets—Detailed Flow Measurements," AIAA Paper 2004-0751, Jan. 2004.

[8]Rixon, G. S., and Johari, H., "Development of a Steady Vortex Generator Jet in a Turbulent Boundary Layer," *Journal of Fluids Engineering*, Vol. 125, Nov. 2003, pp. 1006–1015.

[9]Johari, H., and Rixon, G. S., "Effects of Pulsing on a Vortex Generator Jet," *AIAA Journal*, Vol. 41, No. 12, 2003, pp. 2309–2315.

[10]Postl, D., Gross, A., and Fasel, H. F., "Numerical Investigation of Low-Pressure Turbine Blade Separation Control," AIAA Paper 2003-0614, Jan. 2003.

[11]Postl, D., Gross, A., and Fasel, H. F., "Numerical Investigation of Active Flow Control for Low-Pressure Turbine Blade Separation," AIAA Paper 2004-0750, Jan. 2004.

[12]Bons, J. P., Sondergaard, R., and Rivir, R. B., "The Fluid Dynamics of LPT Blade Separation Control Using Pulsed Jets," *Journal of Turbomachinery*, Vol. 124, No. 1, Jan. 2002, pp. 77–85.

[13]Volino, R. J., "Separation Control on Low-Pressure Turbine Airfoils Using Synthetic Vortex Generator Jets," *Journal of Turbomachinery*, Vol. 125, No. 4, 2003, pp. 765–777.

[14]Khan, Z. U., and Johnston, J. P., "On Vortex Generating Jets," *International Journal of Heat and Fluid Flow*, Vol. 21, 2000, pp. 506–511.

[15]Volino, R. M., and Hultgren, L. S., "Measurements in Separated and Transitional Boundary Layers Under Low-Pressure Turbine Airfoil Conditions," *Journal of Turbomachinery*, Vol. 123, No. 2, 2001, pp. 189–197.